Subsecond Proton-Hole Propagation in Bacteriorhodopsin

Bettina Schätzler,† Norbert A. Dencher,† Joerg Tittor,‡ Dieter Oesterhelt,‡ Sharon Yaniv-Checover,* Esther Nachliel,* and Menachem Gutman*

*Laser Laboratory for Fast Reactions in Biology, Department of Biochemistry, Tel Aviv University, Israel; †Department of Biophysics, Technical University of Darmstadt, Darmstadt, Germany; and ‡the Max-Planck-Institute for Biochemistry, Martinsried, Germany

ABSTRACT The dynamics of proton transfer between the surface of purple membrane and the aqueous bulk have recently been investigated by the Laser Induced Proton Pulse Method. Following a Δ-function release of protons to the bulk, the system was seen to regain its state of equilibrium within a few hundreds of microseconds. These measurements set the time frame for the relaxation of any state of acid-base disequilibrium between the bacteriorhodopsin's surface and the bulk. It was also deduced that the released protons react with the various proton binding within less than 10 μs. In the present study, we monitored the photocycle and the proton-cycle of photo-excited bacteriorhodopsin, in the absence of added buffer, and calculated the proton balance between the Schiff base and the bulk phase in a time-resolved mode. It was noticed that the late phase of the M decay (beyond 1 ms) is characterized by a slow (subsecond) relaxation of disequilibrium, where the Schiff base is already reprotonated but the pyranine still retains protons. Thus, it appears that the protonation of D96 is a slow rate-limiting process that generates a "proton hole" in the cytoplasmic section of the protein. The velocity of the hole propagation is modulated by the ionic strength of the solution and by selective replacements of charged residues on the interhelical loops of the protein, at domains that seems to be remote from the intraprotein proton conduction trajectory.

INTRODUCTION

Illumination of bacteriorhodopsin (BR) generates an electrochemical proton gradient across the purple membrane (PM) by vectorial translocation of a proton during the catalytic cycle. The sequence of spectroscopic changes associated with the catalytic cycle of bacteriorhodopsin has been thoroughly investigated, leading to a generally accepted model that is based on the spectral properties of the retinal-Schiff-base chromophore. It consists of a linear sequence of intermediates labeled J, K, L, M, N, and O, with characteristic absorption maxima. The minimal model of vectorial proton transfer consists of three reversible events and therefore six steps to complete the catalytic cycle. The initial step in the photocycle is light-induced isomerization (photoisomerization (J*)) of all-*trans* retinal to its 13-*cis* configuration. The chromophore then passes through the short-living K and L intermediates before the Schiff base is deprotonated during the L to M transition by proton transfer (T) to D85 involving a charge redistribution among residues (D212, K216, D85, and R82) at the immediate surrounding of the retinal (Dioumaev et al., 1999; Zscherp et al., 2001). This reaction is accompanied by a shift in the absorption maximum of the chromophore to ~410 nm, characterizing the deprotonated state of the Schiff base. During the transition between the substates of the M intermediates (M_1, M_2) (Lanyi, 1992; Varo and Lanyi, 1991a,b). The unprotonated Schiff base redirects its orientation from the extracellular to the cytoplasmic half of the proton channel (switch S). The Schiff base regains its protonated state in the subsequent M to N transition by abstracting a proton (proton transfer T) from D96 (Gerwert et al., 1989), which is the only chargeable moiety in the cytoplasmic half of the channel. The reisomerizaton of the chromophore (isomerization I) proceeds during the transition from state N to O. In the last spectrally observed transition (O to BR), the proton is released from D85 and reprotonates the extracellular proton releasing domain, made of E194, E204, and one or more water molecules (Luecke et al., 2000; Misra et al., 1997; Rammelsberg et al., 1998; Richter et al., 1996; Zscherp et al., 1999). The necessary reset of the proton accessibility to the extracellular surface (switch S) occurs between the N and the initial BR state.

In the present study we shall refer to the deprotonated state of D96 as a ''proton hole,'' and study how a proton coming from the bulk is filling up this deficit. Reprotonation of D96 occurs during or after the N-intermediate, yet this carboxylate is so far from the Schiff base that its protonation state does not affect the protein's absorption spectrum. Therefore, reprotonation of D96 cannot be directly observed by visible absorption spectroscopy but inferred from monitoring the proton abstraction from the bulk phase using a pH indicator. The most probable proton donor to D96 is D38, which in its turn is protonated by D36, a residue that is fully exposed to the bulk. The distance between these proton binding sites is ~12 Å for the initial step, D96→Schiff base, ~9.5 Å for D38→D96, and 6.3Å for the proton transfer from D36 to D38. The reaction of D36 with bulk protons is a fast, diffusion-controlled reaction. The mechanism of the proton propagation along this set of temporary proton binding sites is the subject of the present study.

As will be shown below, the hole propagation toward the cytoplasmic surface caused by deprotonation of D96 is

Submitted August 1, 2002, and accepted for publication September 17, 2002.

Address reprint requests to Menachem Gutman, George S. Wise Faculty of Life Sciences, Tel Aviv University, Ramat Aviv 69978, Israel. Phone 972-3-640-9875; Fax: 972-3-640-6834; E-mail: me@hemi.tau.ac.il.

0006-3495/03/01/671/16 $2.00

a rather slow process, lasting in some mutants up to 1 s. Such a slow passage implies that the rate-limiting step of the reaction is a structural fluctuation in the protein, leading through one or more steps to the protonation of D96 at the expense of deprotonation of D38 (Riesle et al., 1996), which is located near the cytoplasmic surface. The protonation of D38 is a fast and complex reaction, where both D36 and a cluster of three carboxylates on the cytoplasmic surface (D104, E161, and E234; Checover et al., 2001, 1997) assist in the reaction. Thus, it appears that the protein's surface does not only serve as a coating of the protein's functional matrix, but itself functions as an active element by bulk-surface proton transfer reactions.

The indicator of choice for monitoring the dynamics of bulk-surface proton transfer is pyranine (ΦOH) that, due to its negative charge ($Z = -3$ or -4, depending on its state of protonation) is not adsorbed to the net negatively charged purple membrane's surface. Pyranine is also an efficient excited-state proton emitter, suitable for perturbing the bulk-surface protonation equilibrium by injecting free protons into the solution (Checover et al., 2001, 1997; Nachliel et al., 1997; Sacks et al., 1998).

The process of proton transfer between the protein's surface and the mobile indicator in the bulk follows two pathways. One process consists of dissociation of the proton from a donor residue and its diffusion-controlled reaction with various acceptors. In most cases, the rate-limiting step of this pathway is the dissociation of the proton donor. The alternative mechanism, which operates in parallel, is a collisional proton-transfer reaction between the pyranine molecule and the membrane surface. The rate-limiting step for this mechanism is the collision between the reactants (Gutman and Nachliel, 1995). The velocity of the collisional pathway varies with the concentration of the reactants, their diffusivity, and the accessibility of the protonated sites on the protein. In previous studies (Checover et al., 2001; Yaniv-Checover, 2002) we investigated the rate constants of the two pathways and concluded that, through the operation of the two pathways, the equilibrium between the bulk and the surface of bacteriorhodopsin is fully established within 100–200 μs. The relative dominance of each pathway varies with time as a function of the reactants' concentrations. A high concentration of either an indicator or a mobile buffer enhances the contribution of the collisional mechanism to the overall rate of reaction. The analysis of the proton pulse experiments yielded the rate constants for proton transfer reactions between pyranine and the various proton-binding sites of bacteriorhodopsin. Accordingly, these very same rate constants can determine the proton exchange reactions between the pyranine and the protein during the photocycle.

In the present study, we focused our attention on the last steps of the catalytic cycle, and noticed a slow relaxation of a state of disequilibrium between two well-defined chromophores: the unprotonated Schiff base (monitored at 412 nm) and the protonated pyranine in the bulk (monitored at 458 nm). For a rather long time (10–100 ms), the amount of protons, stored in the form of ΦOH, exceeded the capacity of the deprotonated Schiff base to accept them. The relaxation of the disequilibrium was orders-of-magnitude longer than the bulk-surface equilibration time, suggesting that the rate-limiting step of the relaxation was associated with an intraprotein proton transfer reaction from a bulk-accessible donor to the deprotonated D96. To indicate that the mechanism of this reaction is the compensation of a deprotonated reservoir located inside the protein by a donor that is in equilibrium with the bulk, we refer to the process as proton-hole propagation to the cytoplasmic surface of the protein. The protein matrix is spaced between D96 and D38 and consists of hydrophobic residues through which the proton must propagate; it was termed ''hydrophobic gate'' (Dencher et al., 1992).

The slow proton-hole propagation was detected with the WT protein, and in a more pronounced mode, with some mutants in which charged surface residues, located far from the proton-pumping channel, were mutated to uncharged ones. These observations indicate that a minor modulation of the charge distribution on the exposed loops connecting the transmembrane helices is sufficient to cause aberrations in the conformational changes that are essential for the normal operation of the photocycle. To validate whether replacement of a charged residue on the loops can alter the structure of the protein, the very same mutants, whose photocycle was measured, were subjected to a brief proton pulse and the μs reprotonation dynamics of the pyranine anion was subjected to a rigorous kinetic analysis (Checover et al., 2001). These experiments demonstrate that the mutations affect the pK values and the kinetic properties of the bacteriorhodopsin's proton-binding sites while still in its BR ground state.

MATERIALS AND METHODS

Mutants

Site-specific mutants of bacteriorhodopsin were prepared according to Pfeiffer et al. (1999). The codon of any requested position was changed to TGC coding for cysteine by means of site-directed mutagenesis by overlap extension. The PCR product was cloned in the shuttle vector pUS-MEV. Mutagenesis was followed by transformation and homologous expression in *Halobacterium salinarum* strain SNOB (Pfeiffer et al., 1999). Mutated proteins were isolated as purple membrane sheets according to Oesterhelt and Schuhmann (1974). To avoid oxidation of the thiol group, β-mercaptoethanol was present during the lysis of the cells and all subsequent steps at a concentration of 5 mM.

Photocycle measurements

The purple membranes were kept frozen (−80°C) in a solution containing buffer and reducing agent to prevent the oxidation of the cysteine. Before use, the membranes were washed three times by centrifugation using either ultra-pure water or 150 mM KCl. The membranes were then dispersed to a final concentration of 0.1–0.4 mg/ml.

The measurements were carried out within 2 h of the washing procedure in the presence of 20 μM pyranine, pH = 7.5, at 25°C.

The extinction coefficients used for calculating the concentrations of the pyranine and the BR state were 20,000 $M^{-1}cm^{-1}$ (459 nm) and 63,000 $M^{-1}cm^{-1}$ (568 nm), respectively. The differential extinction coefficient for the M state $(\varepsilon_M-\varepsilon_{BR})_{412nm}$ was taken as 34,300 $M^{-1}cm^{-1}$.

Proton pulse measurements

The experiment consists of a Δ-function perturbation of the acid-base equilibrium in the membrane suspension, attained by a UV laser pulse. (For details, see Checover et al., 2001, 1997.) Following the relaxation of the dye to the ground state ($\tau \sim 5$ ns), the system is poised in a temporary state of disequilibrium, wherein both free protons and ΦO^- concentrations are above the equilibrium level, while the ΦOH population is transiently depleted. This initial perturbation propagates to all other proton-binding sites present in the pulsed solution through diffusion-controlled reactions with the photo-dissociation products (H^+ and ΦO^-). The response of the system to the perturbation proceeds through many parallel pathways, where the velocity of each reaction is determined by the concentrations of the reactants and the respective rate constants. The kinetic and stoichiometric coupling between all reactants implies that a followup of one reactant would yield information concerning the state of protonation of all others.

Proteins, as polyelectrolytes, are thermodynamically coupled, and the charging of any site affects the *pK* value of all others (Tanford, 1957; Tanford and Roxby, 1972). Thus, when a large proton pulse challenges a protein, its thermodynamic and kinetic characteristics may vary during the reaction time. To avoid these complications, the experiments were carried out under strict restrictions where the incremental proton concentration was smaller than the total protein concentration, ensuring that each protein molecule reacts with no more than a single proton.

The instrumental setup for the photocycle and proton transfer measurements

The optical geometry and electronic setup were as previously described in Checover et al. (2001). Pyranine (8-hydroxy-pyrene-1,3,6-trisulfonate, laser grade) was purchased from Eastman Kodak (Rochester, NY).

Preparation of the sample

Purple membranes were extensively washed with pure water by three repeated centrifugations to remove buffers and the reductant. Finally the membrane was suspended as a concentrated suspension, either in water or in 150 mM KCl, and diluted to the desired concentration inside the measuring cell.

The proton pulse experiments were carried out within 2 h of the washing procedure, using varying concentrations of protein (3–20 μM with respect to the retinal concentration) or pyranine (20–30 μM) at 25°C. The pH of the measurements was varied within the pH range of 6–8 and at each pH, the kinetics were measured both at 4 and 20 μs/div. The measured signals are an average of 1024 traces.

Kinetic analysis of the absorbance signals after Laser Induced Proton Pulse Method

The experimental curves were analyzed by a detailed reconstruction of the dynamics of all chemical reactions that are affected by the acid-base perturbation. (For details, see Checover et al., 2001.)

RESULTS

The photocycle of WT bacteriorhodopsin

The transient formation of the M state and the corresponding depletion of the absorbance at 568 nm, representing the ground state, as measured for the WT bacteriorhodopsin, are depicted in Fig. 1 *A*. The formation of the M state is characterized by a fast rise time ($\tau < 100$ μs), while the decay is significantly slower and extends over the ms time range. Fig. 1 *B* depicts the transient protonation of the pyranine anion, added to the solution as a pH indicator. In the absence of another proton acceptor, any proton released from the protein should be present either as a free diffusing one bound to the dye, or to some residues on the PM. As will be shown below, after a Δ-function proton pulse, the free proton concentration relaxes to the prepulse level within a few μs. As the photocycle lasts many ms, the contribution of the free protons to the total proton balance is limited to the most initial phase of the observation and at any time point later than a few μs, the free proton concentration can be ignored.

Comparison between the dynamics of the reversible deprotonated Schiff base (M), and the transient protonated pyranine, both expressed in molar units as measured in the absence of the screening electrolyte, reveals a difference both in the time constants and in amplitudes. Apparently, only ~50% of the protons released from the Schiff base reacted with the indicator during the photocycle, whereas the rest of the released protons reacted with the various proton-binding sites on the protein's surface. Due to these reactions, which affect the ΦO^- concentration but not the protonation state of the Schiff base, the time constants of the pyranine's protonation and the dynamics of the M state are not the same. Repetition of the same experiment in the presence of a screening electrolyte (150 mM KCl; see Fig. 1 *A*, *dashed line*) demonstrates that the BR and the M dynamics are unaffected by the addition of the electrolyte, yet the amount of protonated pyranine (Fig. 1 *B*) was significantly increased: up to ~70% with respect to the amount of protons released from the Schiff base. It should be mentioned that in absorbance measurements, the protonation of the pyranine is recorded as a decrement of the ΦO^- concentration. For this reason, the transient protonation of the pyranine is presented with the polarity of the experimental observations, as a negative signal. The ratio of the time constants of the kinetics of protonation and deprotonation of pyranine in water and in salt reflects the easier dispersion of protons between the surface and the bulk, leading to a twice-faster protonation and a twice-slower deprotonation of pyranine in 150 mM KCl as compared to the measurements in water. The apparent enhancement is attributed to ionic screening that facilitates the dispersion of the protons from the surface toward the bulk. Thus, whereas the quantitation of the amount of moles of protein that had lost their Schiff base's protons is feasible, a positive identification of the protonated sites on the protein, except for the Schiff base, is unattainable.

In the present study, we shall focus on the comparison between the residual concentration of the nonprotonated Schiff base ($M_{(t)}$ measured at 412 nm), and the increment of the protonated pyranine at the same time point ($\Phi OH_{(t)}$).

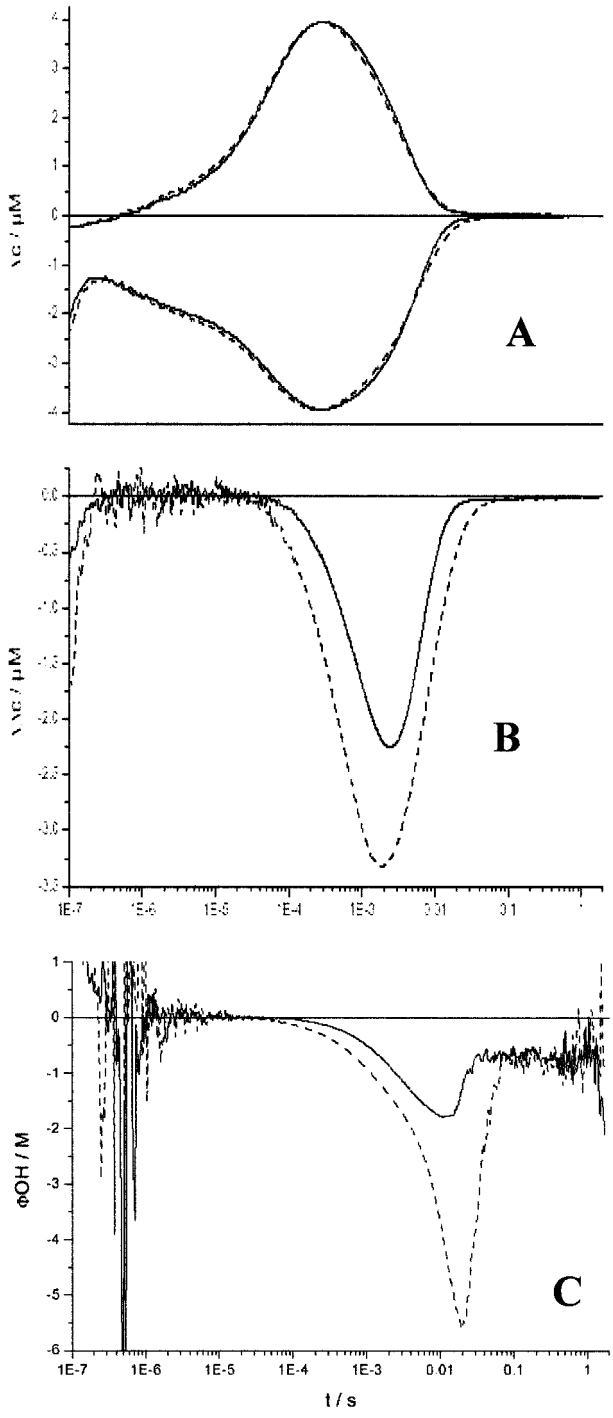

FIGURE 1 (*A*) Flash-induced transient concentration changes of the M-intermediate at 412 nm (*upper trace*) and the ground state at 568 nm (*lower trace*). (*B*) The transient protonation of pyranine, as measured at 459 nm. (*C*) Depicts the ratio of the residuals $\Delta\Phi OH_t/\Delta M_t$ as a function of time. The measurements were carried out with the WT bacteriorhodopsin in water (—) and 150 mM KCl (- - - -). The reactants concentrations were $PM = 0.364$ g/L, $\Phi OH = 20\ \mu$M, $T = 25°$C, $pH = 7.5$. It should be noted that the incremental protonation of the pyranine was corrected for the signal recorded in its absence, reflecting a minor contribution of the chromophore at the wavelength where the pyranine was measured. For this reason the ordinate in *B* is marked as $\Delta\Delta C$. The amplitude is presented as a negative signal in accordance with the direction of the absorbance transient.

Examination of the residuals at the 10-ms time point reveals that, whereas the reprotonation of the Schiff base is almost identical in the absence or presence of the screening electrolyte ($M_{(t)} = 0.33$ and 0.38 μM, respectively), the residual ΦOH at that time is significantly higher than the residual M state, and the discrepancy increases in the presence of a screening electrolyte, 0.6 and 1.4 μM of ΦOH, respectively. Namely, the reprotonation of the Schiff base proceeds faster than the proton transfer from the bulk to the protein.

The discrepancy between the two measured parameters $\Delta\Phi OH_t$ and ΔM_t is best demonstrated in frame C, where the incremental concentration of protonated pyranine at time t ($\Delta\Phi OH_t$), divided by the amount of protons missing at that time point from the Schiff base (ΔM_t) is plotted as a function of time. In the short time range, where both amplitudes are small, the ratio is close to zero and exhibits a large noise. With time, the ratio become large and the curve is much smoother. With longer time, the ratio declines and fades into a noisy region, where both parameters become small. Once the ratio is higher than 1, the number of protons released from the Schiff base exceeds the number of deprotonated Schiff base present in the solution. Considering the mass conservation law, we must conclude that, at that time range, the Schiff base had been already protonated by D96, yet the local proton deficit had not been compensated by a bulk proton. When measured in water, the ratio $\Delta\Phi OH_t/\Delta M_t$ is as large as ~1.6 and attains its maximal value at ~10 ms. In the presence of a screening electrolyte, it is as high as 5.7 and the maximum is slightly delayed in time.

It should be emphasized that our previous studies on the rate of bulk surface equilibration revealed that an acid-base disequilibrium between the two phases relaxes within less than 250 μs (Checover et al., 2001; and see below). Consequently, the temporal discrepancy between the residual kinetics of $M_{(t)}$ and $\Phi OH_{(t)}$ should be interpreted by implicating the rate of the intraprotein proton transfer as the cause for the transient disequilibrium.

Time-resolved measurements of bulk-surface proton transfer reactions

The transient protonation of WT bacteriorhodopsin was measured by Laser Induced Proton Pulse Method (LIPPME) in the presence and absence of 150 mM KCl, and subjected to a kinetic analysis. The analysis is consistent with the dynamics calculated for the presence of five proton attractors, namely the pyranine anion, the carboxylates of D36 and D38 (these residues differ in their rate constants and pK values), a cluster of three carboxylates present on the cytoplasmic surface of the membrane, and a single carboxylate located on the extracellular surface (for details, see Checover et al., 2001).

The rate constants and pK values of the proton binding sites, measured either in pure water or in 150 mM KCl, are listed in Table 1.

TABLE 1 The kinetic and thermodynamic parameters characterizing the WT bacteriorhodopsin membrane. The table compiles kinetic analysis of 35 independent kinetic observations, carried out with the WT protein under varying initial conditions (pH, ionic strength, protein, and pyranine concentrations)

			pK		Site + H^+ ($M^{-1}s^{-1}$)		Site + ΦO^- ($M^{-1}s^{-1}$)	
Site	*n**	side	Water	150 mM KCl	Water	150 mM KCl	Water	150 mM KCl
ΦO^-	–	–	7.7 ± 0.1	7.6 ± 0.05	7.3 (± 0.4) × 10^{10}	5.4 (± 0.5) × 10^{10}	—	—
D36	1	Cyt	4.5 ± 0.4	4.5 ± 0.4	1.5 (± 0.2) × 10^{10}	1.0 (± 0.1) × 10^{10}	≤ 5.0 × 10^8	≤ 1.0 × 10^8
D38	1	Cyt	6.5 ± 0.1	6.5 ± 0.1	0.5 (± 0.1) × 10^{10}	0.4 (± 0.05) × 10^{10}	≤ 3.0 × 10^8	≤ 2.0 × 10^8
Cluster	3	Cyt	5.5 ± 0.05	5.4 ± 0.06	4.0 (± 0.6) × 10^{10}	2.9 (± 0.2) × 10^{10}	4.0 (± 0.3) × 10^9	5.2 (± 0.7) × 10^9
COO_{ext}	1	Ext	5.1 ± 0.3	5.1 ± 0.3	0.5 (± 0.3) × 10^{10}	0.5 (± 0.3) × 10^{10}	9.0 (± 0.5) × 10^9	9.0 (± 0.5) × 10^9

*n**, the number of moieties that constitute the proton binding site.

As emerges from Table 1, the main effect of the salt is to slow down, by ~25%, the diffusion-controlled reactions between the free protons and the dye, and the carboxylates' cluster on the cytoplasmic surface. This effect is readily explained by the screening effect that lowers the electrostatic attraction between the free proton and the negatively charged acceptor. In parallel, the rate constants of the collisional proton transfer between the cluster and the pyranine anion increased by 25%. This effect is also in accord with the expected effect of the ionic screening on the encounter of the pyranine molecule (Z = −3; −4 depending on its state of protonation) with the negatively charged protein's surface. The rate constants characterizing the external carboxylate residue remain constant. Please note that the site identified as D38 has a somewhat limited accessibility to free proton and it hardly reacts with the pyranine anion. Yet, even a rate constant of 4 × 10^9 $M^{-1}s^{-1}$ is within the range of diffusion-controlled reactions.

As seen in Fig. 2, the protonation reactions of the protein's proton-binding sites are extremely fast. The cluster attains its maximal level of protonation within less than 5 μs, whereas for D38, where the process is a little slower, maximal protonation is attained at ~15 μs. The proton-binding capacity of D36, because of its lower *pK*, is rather small and its transient protonation is observed only on expansion of the *y*-axis (*see inset*). The relaxation of the free proton population is extremely fast and within less than 3 μs, the free proton concentration is almost identical with the prepulse level. The rapid uptake of the free protons by the various proton-binding sites present in the reaction mixture implies that the relaxation of the system proceeds, almost exclusively, by collisional proton transfer reaction between the pyranine anion and the proton binding sites on the protein. The signals measured in 150-mM electrolyte, and their subsequent analysis, revealed a practically identical pattern.

It should be stressed that, independent of the presence of the screening electrolyte, the perturbation had relaxed to merely ~2% of the initial amplitude within less than 250 μs. Thus, while monitoring the proton balance between the purple membranes and the pyranine in the bulk, any state of bulk-protein disequilibrium that extends beyond the ms time point implies that the rate-limiting step of the process involves an intraprotein proton transfer.

The fast relaxation of the free proton population has a direct implication on the present study, as it allows a crucial approximation which is essential for the proton balance calculations; at any given time, which is more than 5 μs past the proton's ejection to the bulk, we can assume that the proton will be bound either to the pyranine or to the protein. Accordingly, Eq. 1 expresses the proton balance at any given time:

$$\Delta M_{(t)} - \Delta \Phi OH_{(t)} = \Delta H^+_{\text{protein(t)}} \quad (1)$$

where $\Delta M_{(t)}$ is the amount of protons that are still detached from the Schiff base, $\Delta \Phi OH_{(t)}$ is the amount of protons bound to the pyranine in the bulk, whereas the difference between the two quantities ($\Delta H^+_{\text{protein(t)}}$) is equal to the amount of protons that are bound to all other proton-binding sites present in the system (bacteriorhodopsin and the anionic sites of the membranal lipids). When $\Delta M_{(t)}$ is smaller than $\Delta \Phi OH_{(t)}$, the $\Delta H^+_{\text{protein(t)}}$ becomes negative, meaning that

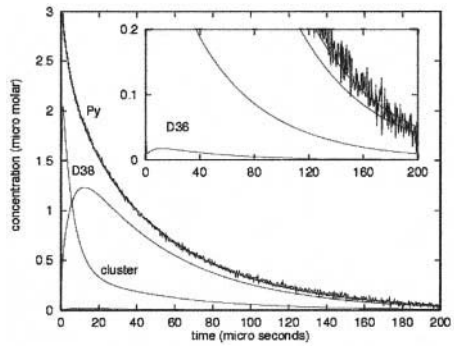

FIGURE 2 Dynamics of reprotonation of pyranine anion as measured in the presence of WT bacteriorhodopsin in pure water. The main frame depicts the decay of the incremental pyranine anion together with the reconstructed curves of the experimental signal (marked in Figure as *Py*) for the cluster and D38. The relaxation of the carboxylate of D36 is hardly observed in the main frame and presented, in an expanded *y*-scale, in the inset. Signals that were measured in 150 mM KCl yielded almost identical decay dynamics and the rate constants reconstructing these experimental curves are given in Table 1.

somewhere in the protein there are site(s) which are in a temporary state of disequilibrium with the bulk.

The effect of replacement of charged surface residues on the photocycle

Fig. 3 depicts the photocycle traces of the WT protein and of nine mutants where a charged residue, located far from the immediate vicinity of the Schiff base, was replaced by cysteine or glutamine. Traces in the right panels were recorded in the presence of a screening electrolyte, whereas the left panels show traces recorded in pure water. Fig. 3 *A* (*top panels, left* and *right*) depict the dynamics measured at 412 nm, where the M state is characterized by a differential extinction coefficient of $\Delta\varepsilon_M = 34300\ M^{-1}\text{cm}^{-1}$.

The transients, as measured with the various mutations, differed in initial *PM* concentration, and for proper comparison, all signals were normalized according to the WT absorbance at 568 nm, taking the WT as a reference. The protonation of the pyranine (*B*, *left* and *right*) was measured at 459 nm, which, within the experimental accuracy, is an isosbestic point with respect to the color changes of the protein's chromophore.

The concentrations of the protonated pyranine are consistently smaller than the M signal and exhibit a large variation in amplitude and relaxation time. The low yield of protonated indicator is attributed to the binding of protons to various sites on the purple membrane, which compete with the pyranine anion for the free proton. The addition of the screening electrolyte apparently increased the yield of ΦOH in most cases, yet for two mutants (D104C, *cyan*; R227Q, *gray*), the amplitudes of the pyranine signals were decreased. The fact that the screening electrolyte can either increase or decrease the amplitude of ΦOH implies a complex

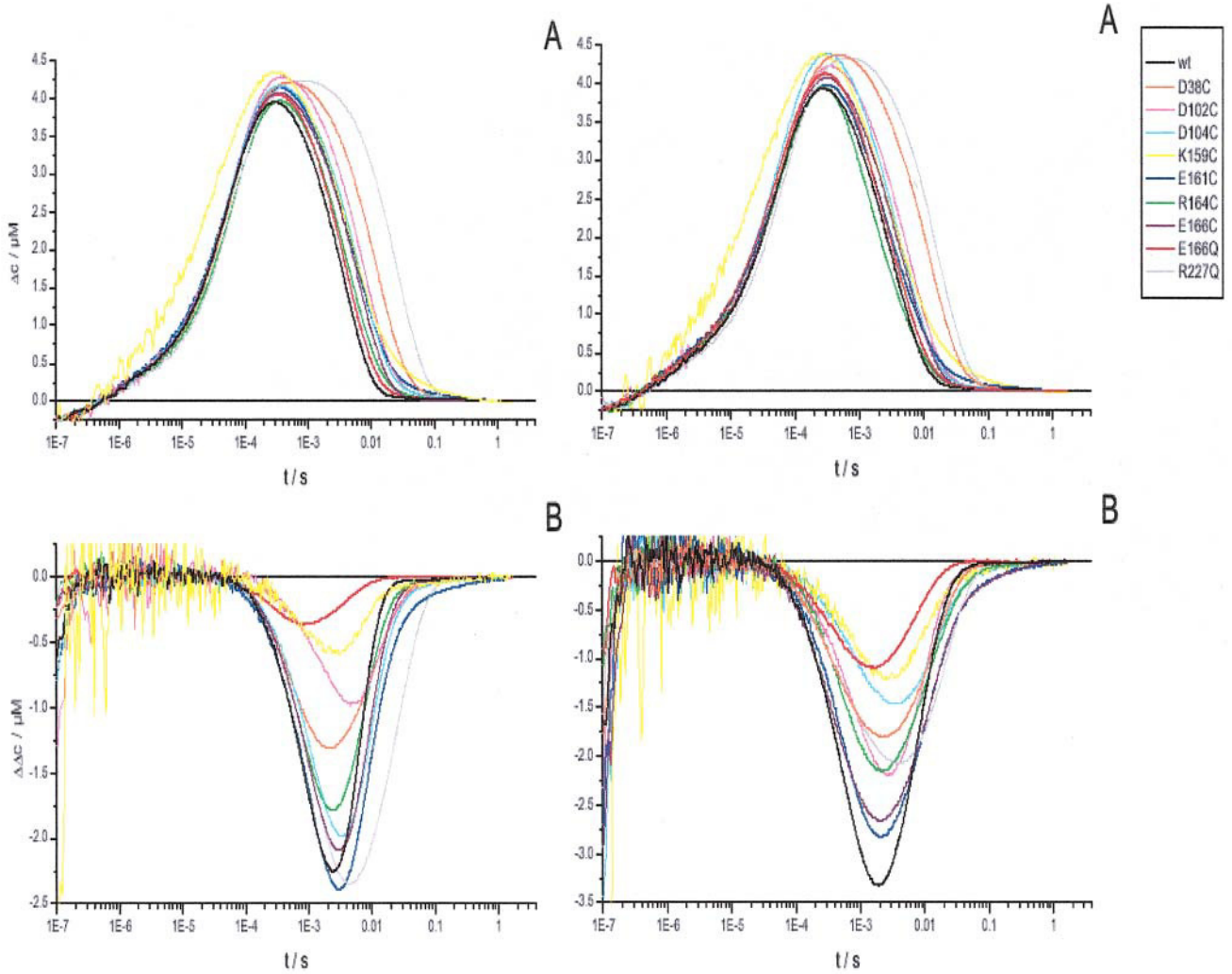

FIGURE 3 Flash-induced transient concentration changes of the M-intermediate at 412 nm (*top frames*) and of pyranine at 459 nm (*lower frames*) of WT bacteriorhodopsin and BR mutants D38C, D102C, D104C, K159C, E161C, R164C, E166C, E166Q, and R227Q ($T = 25°C$, $pH = 7.5$). (*Left panel*) The measurements were carried out in pure water. (*Right panel*) The measurements were carried out in 150 mM KCl.

correlation between the nature of the mutation and affects the intraprotein proton transfer mechanism. Because of the adjustment procedure used in Fig. 3, internal normalization of $\Delta\Phi OH_t/\Delta M_t$ as in Fig. 1 *C*, will be used below (Fig. 7) for the precise analysis of the signal.

The time constant and amplitudes of the main component of the M dynamics (rise and decay) and the apparent time constant of the pyranine's deprotonation were calculated and their values listed in Table 2 *A* and *B*, respectively. The M rise of all tested proteins was fast, 50–100 μs, and varied between the mutants within less than twofold. Except for the dynamics measured with K159C, where the M formation was significantly faster than all other samples, we consider the measured variability as insignificant. Apparently, the replacement of charged residues on the cytoplasmic side had a marginal effect on the dynamics of internal proton ejection to the extracellular surface of the membrane and to the bulk. The M decay of all proteins was ~50- to 100-fold slower than its rise and varied between the mutants from ~4 ms (measured with the WT) up to ~30 ms (R227Q). The pyranine dynamics exhibit a large variation in the apparent time constant of deprotonation, varying by up to fivefold (R227Q) with respect to the time constant measured with the WT.

Although the screening electrolyte has a marginal effect or a slight acceleration on the M decay, its addition significantly delayed the relaxation of the pyranine dynamics (values in parenthesis; last column of Table 2 *B*). The fact that a screening electrolyte can slow down the deprotonation of the pyranine but hardly affects the reprotonation of the Schiff base indicates that the two processes are not inherently coupled. The M decay corresponds to a proton transfer from the carboxylate of D96 to the Schiff base, leaving a proton hole inside the cytoplasmic proton channel of the protein.

Quantitative expression of the proton hole is attained by direct comparison between the residuals (in molar units) of the M state and ΦOH at 10 ms. This time point was selected as it is orders-of-magnitude later than the time when the bulk-surface equilibration occurs, and all exposed proton-binding sites had ample time to equilibrate with the bulk. The comparison between the residuals at the 10-ms time point is given in Table 3.

Columns 2 and 3 in Table 3 list the residuals of M state and ΦOH as measured in water. In the case of the WT and one mutant (E161C) we notice a significant excess of ΦOH over the M concentration. When the screening electrolyte is present (columns *4* and *5*), the excess of ΦOH over M state is prevalent with the WT and with E161C and also seen in four more mutants (D102C, D104C, R164C, and E166C) (see **bold** numbers in the Table).

In the remainder of the mutants, at the 10-ms time mark, the value of $\Delta\Delta\Phi OH_{(t)}$ was found to be lower than $\Delta M_{(t)}$. The source of this observation can be attributed to a variation of the proton-binding capacity of the surface of the mutated proteins, and to partial aggregation of the purple membranes, topics that may merit research. In the present study we shall

TABLE 2 Time constants and amplitudes for the rise and decay of the M-intermediate and deprotonation of pyranine of WT bacteriorhodopsin and BR mutants as measured in (*A*) pure water and (*B*) in 150 mM KCl ($T = 25°C$, $pH = 7.5$)

A

Water	$\tau_{M\ rise}$ (μs)	$A_{M\ rise}$/OD	$\tau_{M\ decay}$ (ms)	$A_{M\ decay}$/OD	$\tau_{pyranine\ deprotonation}$ (ms)
WT	68.1	−0.1344	3.7	0.1476	4.3
D38C	78.2	−0.1544	13.2	0.1723	12.9
D102C	72.1	−0.0330	8.0	0.0363	12.5
D104C	66.3	−0.1100	6.9	0.1190	9.4
K159C	47.2	−0.0350	6.1	0.0405	6.5
E161C	65.8	−0.1124	6.4	0.1212	10.0
R164C	75.8	−0.1532	4.9	0.1653	7.2
E166C	65.9	−0.1306	6.3	0.1434	7.9
E166Q	72.6	−0.1554	4.3	0.1725	4.1
R227Q	94.2	−0.1652	28.3	0.1883	27.3

B

150 mM KCl	$\tau_{M\ rise}$ (μs)	$A_{M\ rise}$/OD	$\tau_{M\ decay}$ (ms)	$A_{M\ decay}$/OD	$\tau_{pyranine\ deprotonation}$ (ms)
wt	60.7	−0.1313	3.5 (0.95)*	0.1437	**8.8 (2.0)***
D38C	73.6	−0.1294	12.4 (0.94)	0.1456	15.6 (1.2)
D102C	68.5	−0.0321	6.1 (0.76)	0.0359	9.3 (0.7)
D104C	61.3	−0.0851	4.8 (0.67)	0.0934	**18.2 (1.93)**
K159C	40.1	−0.0263	4.1 (0.67)	0.0305	**12.0 (1.84)**
E161C	61.4	−0.0828	4.1 (0.64)	0.0916	**14.1 (1.4)**
R164C	59.7	−0.0921	2.9 (0.59)	0.0997	**14.6 (2.03)**
E166C	60.4	−0.1645	5.0 (0.79)	0.1810	**15.6 (1.97)**
E166Q	61.6	−0.1001	3.7 (0.86)	0.1128	**8.1 (1.97)**
R227Q	95.3	−0.1650	17.6 (0.62)	0.1923	25.0 (0.92)

*The number in parenthesis denotes the ratio between the relaxation time in the presence of screening electrolyte vs. that measured in pure water.
Bold numbers denote the cases where the deprotonation time of the pyranine signals were at least twice that of the decay measured for the M state.

TABLE 3 Temporal concentrations of the M-intermediate and of protonated pyranine at 10 ms of WT bacteriorhodopsin and BR mutants D38C, D102C, D104C, K159C, E161C, R164C, E166C, E166Q, and R227Q in water, and in 150 mM KCl ($T = 25°C$, $pH = 7.5$)

	Water		150 mM KCl	
	$\Delta M_{(t)}$ (μM)	$\Delta\Delta\Phi OH_{(t)}$ (μM)	$\Delta M_{(t)}$ (μM)	$\Delta\Delta\Phi OH_{(t)}$ (μM)
wt	**0.33**	**0.59**	**0.38**	**1.40**
D38C	2.05	0.75	2.038	1.16
D102C	1.33	0.75	**0.99**	**1.15**
K159C	1.2	0.26	1.04	0.69
D104C	1.12	1.14	**0.82**	**1.13**
E161C	**1.1**	**1.33**	**0.76**	**1.68**
R164C	0.69	0.73	**0.44**	**0.76**
E166C	0.92	1.033	**0.76**	**1.67**
E166Q	0.52	0.04	0.52	0.40
R227Q	3.11	2.02	2.54	1.74

Bold numbers emphasize the case where $\Delta\Delta\Phi OH_{(t)}$ exceeds significantly the value of $\Delta M_{(t)}$.

not investigate the reactions of these mutants where, at the 10-ms time point, $\Delta M_{(t)} > \Delta\Delta\Phi OH_{(t)}$.

It should be emphasized that the detected variation in the hole propagation is affected not only by the site of mutation, but also by the nature of the replacing residue. Thus the two mutants E166C and E166Q markedly differ in the ratio of residuals at the 10-ms time mark. For E166C, $\Delta\Phi OH_{(10\ ms)}$ exceeds that of $\Delta M_{(10\ ms)}$, whereas, with E166Q, the $\Delta\Phi OH_{(10\ ms)}$ is smaller than the residual M concentration.

The effect of replacement of charged surface residues on the dynamics of bulk-surface equilibration

The results presented above may be explained by assuming that the replacement of charged surface residues reduces the rate constants of bulk-surface proton exchange up to the point of creating a rate-limiting step. This hypothesis can be investigated by measuring the dynamics of bulk-surface equilibration whereas the protein retains a constant photocycle state (BR) during the whole length of the observation time. This requirement is met by the LIPPME technique, as used above for evaluation of the effect of the screening electrolyte on the bulk-surface equilibration dynamics. The measurements, which were carried out with the WT protein (Fig. 2 and Table 1), were repeated with each of the mutants. The analysis was carried out by assuming that the mutation had no effect on the pK and kinetic parameters of the surface groups, and the fitting of the signals was attempted by using the parameters of the WT protein. When this failed, the features of the proton binding sites were varied until more than 20 independently measured signals could be fitted within the limits set by the electronic noise by the same set of parameters.

Fig. 4 represents two typical transient absorbance signals that were measured either with E166C or R227Q (Fig. 4, *A* and *B*, respectively). The first mutant exhibits pyranine reprotonation dynamics that are faster than those measured with the WT protein, whereas, in the latter, the reprotonation of the pyranine is slower than the WT dynamics.

As seen in Fig. 4 *A*, the experimental curve relaxes faster than the reconstructed dynamics calculated with the WT parameters for the experimental conditions in which the measurement was carried out. A faster reprotonation of the pyranine anion implies that the mutated protein has a lower capacity, with respect to the WT, to compete with the pyranine anion for free protons.

Table 4 lists the kinetic and thermodynamics parameters characterizing the reactions between free proton and pyranine and the cluster on the cytoplasmic surface of the purple membrane preparation. For sake of brevity, no other parameters were included as they varied within $\pm 20\%$ from the values determined for the WT protein.

As seen in Table 4, the main proton binding site of the protein, the three-carboxylate's cluster (x) on the cytoplasmic surface, is characterized in E166C by a slightly higher pK value, a slower rate of reaction with free protons and an enhanced rate of collisional proton transfer to pyranine. Yet, even the reduced rate constants are sufficiently high to ensure equilibration between bulk and surface in a sub-ms time frame.

The dynamics measured with R227Q are characterized by a slow deprotonation of pyranine (see Fig. 2, and Fig. 5 below). Reaction kinetics of the reversible protonation of this mutant are presented in Fig. 4 *B*. The results obtained with the proton pulse technique reveal that the initial reprotonation of the pyranine, measured with R227Q, is compatible with that of the WT protein (represented by the reconstructed dynamics). Yet, ~5 μs after the laser pulse, the protonation

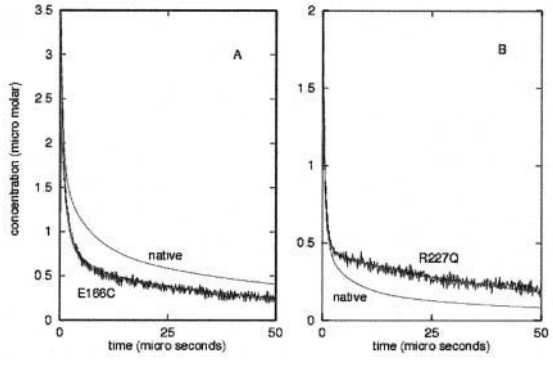

FIGURE 4 Real time measurements of the reprotonation dynamics of photo-excited pyranine in the presence of two mutants of bacteriorhodopsin E166C (*A*) and R227Q (*B*). The measurements were carried out in water at $pH = 7.4$. Each frame depicts the experimental signal of the pyranine reprotonation and the reconstructed signal calculated for the same initial conditions (pH, protein, and pyranine concentration) based on the parameters characterizing the WT protein (marked *native*).

TABLE 4 The effect of replacement of charged surface groups on the thermodynamic and kinetic parameters of bulk-surface proton transfer dynamics

Mutant	N^*	$n^{\#}$	pK	$k_{(X\ +\ H+)}(M^{-1}s^{-1})$	$k_{(XH\ +\ \Phi O-)}(M^{-1}s^{-1})$
WT	57	3	5.5 ± 0.05	4.0 (± 0.65) × 10^{10}	4.0 (± 0.3) × 10^{9}
D102C	22	3	5.5 ± 0.05	5.0 (± 0.9) × 10^{10}	3.0 (± 0.8) × 10^{9}
D104C	26	2	6.5 ± 0.05	3.9 (± 0.9) × 10^{10}	5.0 (± 0.5) × 10^{9}
D38C	17	3	5.5 ± 0.05	1.0 (± 0.5) × 10^{10}	3.7 (± 0.8) × 10^{9}
E161C	18	2	5.5 ± 0.05	4.3 (± 0.5) × 10^{10}	3.4 (± 1.0) × 10^{9}
E166C	40	3	5.8 ± 0.05	2.0 (± 0.6) × 10^{10}	9.0 (± 0.9) × 10^{9}
R164C	45	3	6.0 ± 0.05	2.9 (± 0.4) × 10^{10}	2.6 (± 0.9) × 10^{9}
R227Q	31	3	6.4 ± 0.05	6.2 (± 0.6) × 10^{10}	0.21 (± 0.01) × 10^{9}
K159C	31	2	5.3 ± 0.2	1.0 (± 0.5) × 10^{10}	1.0 (± 0.1) × 10^{9}
		1+1	6.2 ± 0.05	2.7 (± 0.7) × 10^{10}	0.27 (± 0.08) × 10^{9}

N^* denotes the number of independent measurements that were fitted by one set of rate constants.
$n^{\#}$ denotes the number of the residues that constitute the proton binding site.

of pyranine as measured in the presence of the mutant becomes significantly slower than that calculated for the WT protein. The kinetic and thermodynamic parameters characterizing R227Q (Table 4) reveal an increase of the pK of the three-carboxylate cluster, and a 20-fold reduction in the rate constant of proton transfer from the cluster to the dye. It should be pointed out that the 20-fold reduction of the collisional proton transfer is not sufficient to impose a rate-limiting step on the bulk-surface equilibration. When approximating a pyranine concentration of ~10 μM (in accordance with the pH and pyranine concentration used in the measurements) and the rate constant of proton exchange between the cluster and the pyranine ($k = 2 \times 10^{8}$ $M^{-1}s^{-1}$), the time constant of the relaxation will not exceed 500 μs. Even such a slow reaction cannot account for the persistence of the proton hole beyond the 10-ms time point.

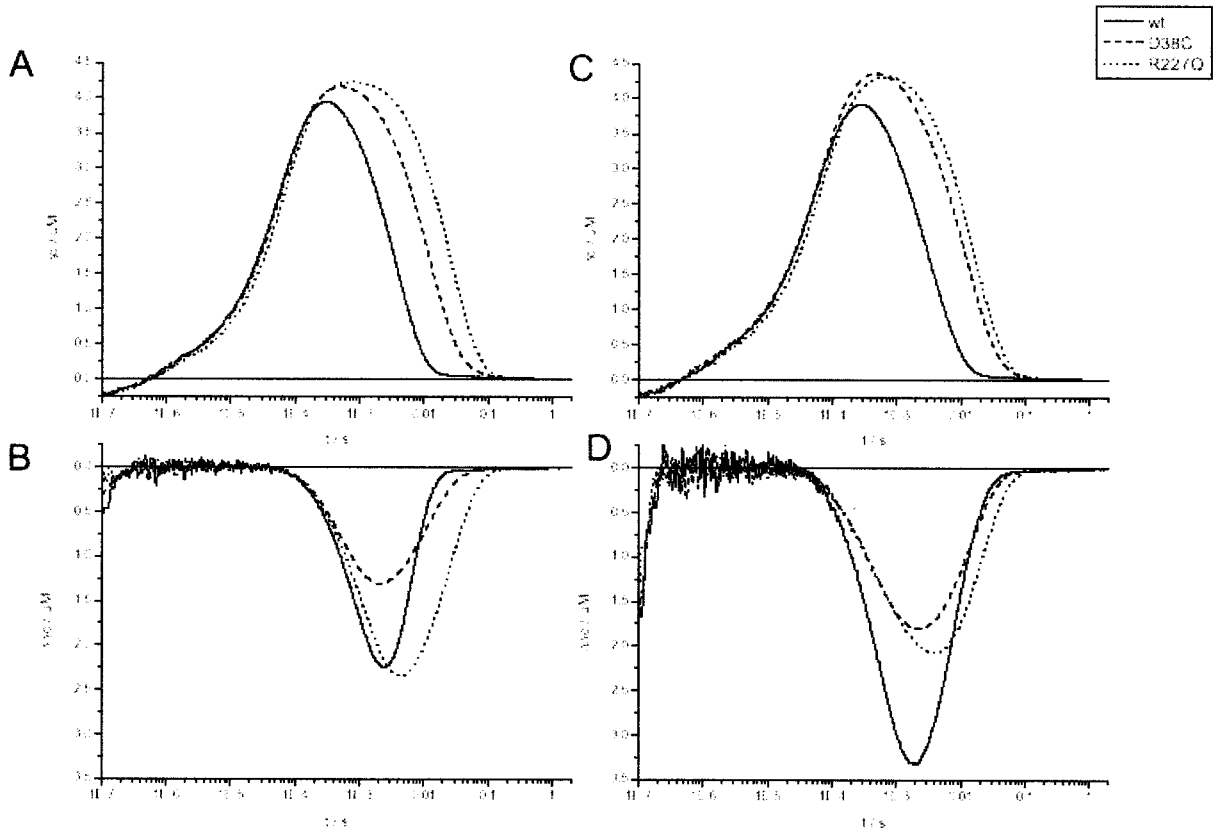

FIGURE 5 Flash-induced transient concentration changes of the M-intermediate at 412 nm (*A*, *C*) and of pyranine at 459 nm (*B*, *D*) of WT bacteriorhodopsin and BR mutants D38C and R227Q in water (*A*, *B*) and in 150 mM KCl (*C*, *D*). The measurements were carried out at $T = 25$°C and $pH = 7.5$).

Close examination of the parameters given in Table 4 reveals that replacement of charged surface groups alters the kinetic and thermodynamic properties controlling the bulk-surface proton transfer of the protein. The mutations can modulate the pK of the three carboxylates cluster (column 4), the rate of reaction of the cluster with free protons or its reaction with the pyranine anion. In the case of K159C, the replacement of a positive charge by cysteine caused a major reorganization of the proton-binding sites on the cytoplasmic surface. Instead of the three-carboxylates cluster, as in the WT protein, this mutant is characterized by a pair of carboxylates ($pK = 6.2$) that react with free protons at a rate constant of $2.7 \times 10^{10}\ M^{-1}s^{-1}$ plus two single non-interacting carboxylates (Checover et al., 2001) having a lower pK and rate of reaction with free proton ($k = 1 \times 10^{10}\ M^{-1}s^{-1}$) that is typical for an isolated carboxylate (Nachliel et al., 1996; Nachliel and Gutman, 1988). Yet, in all these cases, the rate constants are in the order of diffusion-controlled reactions and cannot impose a rate-limiting step that will slow the bulk-surface equilibration. It is an unavoidable conclusion that the lingering of the proton-hole beyond the 10-ms time frame must be due to a rate-limiting step inside the protein.

Mutations affecting both M decay and deprotonation of ΦOH

Two of the mutants reported in this study (D38C and R227Q) exhibited extended decay of the two proton binding chromophores; the Schiff base and the pyranine. These measured signals, as recorded in water and in the presence of 150 mM KCl, are shown in Fig. 5.

The M dynamics of the two mutants in water and in salt (Fig. 5, *A* and *C*) are characterized by a rise time that overlaps the WT dynamics, indicating that the deprotonation of the Schiff base proceeds at a normal rate. The relaxation of the M state is much slower than that of the WT, indicating that in these mutants the proton transfer from the D96 to the Schiff base is delayed. The photocycle of the two mutants is hardly affected by the screening electrolyte.

The dynamics of the pyranine deprotonation in the presence of the mutants, shown in Fig. 5, *B* and *D*, clearly deviate from the WT pattern; the deprotonation of the pyranine extends in time, matching the reprotonation dynamics of the Schiff base, as if the same rate-limiting step controls the two processes. The measurements of the two mutants, in the presence of a screening electrolyte do not exhibit any extension of the relaxation to a longer time frame than in water (in contrast to dynamics measured with the WT) suggesting that, with these mutants, the ionic screening has no delaying effect on the proton passage from the bulk toward D96 as it has for the WT. Unless we reject all the accumulated evidence that D96 is the only proton donor on the cytoplasmic section of the protein that reprotonates the Schiff base in the M state, it must be concluded that the proton transfer between D96 and the Schiff base is the common rate-limiting step for the two events. Once the reprotonation of the Schiff base is sufficiently slow, the proton transfer from the surface groups toward the D96 easily follows up this slower process.

Fig. 6 depicts another type of relaxation dynamics, which was recorded with D102C (Fig. 6 *A*) and E166Q (Fig. 6 *B*). In both mutants the late phase of the ΦOH deprotonation is a mirror image of the reprotonation of the Schiff base, which is also comparable with that of the WT. Thus, although for D38C and R227Q we concluded that the slow relaxation was attributed to a common rate-limiting step, from D96 to the Schiff base, the dynamics measured with D102C and E166Q suggest that the protonation of D96 was accelerated up to the point that it is sufficiently fast to match the D96→Schiff base proton transfer. The two pairs of mutation, D38C and R227Q vs. D102C and E166Q, indicate that the rate constants of proton transfer between D96→Schiff base and D38 →D96 are independent of each other.

Mutations that delay the proton hole propagation with respect to the WT

Fig. 6, *A* and *B*, depict experimental curves measured with D104C, E161C, E166C, and R164C, where the deprotonation of the pyranine extends up to the one second time point, whereas the reprotonation of the Schiff base of these mutants relaxes in dynamics similar to those of the WT. The relaxation curves of the pyranine's deprotonation, recorded in the presence of these mutants, do not follow either a first- or a second-order reaction (data not shown), indicating that the mechanism leading to the slow-hole propagation represents a complex process with possible shifting of the rate-limiting step as a function of time (or the progression of the reaction).

The signals presented in Fig. 6 were normalized, according to their absorbance at 568 nm, with respect to the WT. To evaluate the results in a more quantitative presentation, they are presented in Fig. 7 by the ratio $\Delta\Phi OH_t / \Delta M_t$ vs. time. Thus, when comparing the two mutations, D102C and D104C, which are close to each other and may replace each other in the cluster (Nachliel et al., 2002), the result of their replacement by cysteine on the rate of intraprotein proton transfer is entirely different. The mutant D102C exhibits a fast proton transfer toward D96, as the maximal $\Delta\Phi OH_t / \Delta M_t$ ratio is lower than in the WT, inasmuch as the replacement of the carboxylate of D104 causes a large delay of the proton transfer and the ratio is as large as 3. In the same sense, the data presented in Fig. 7 *B* indicates that the replacement of the same residue (E166) by either cysteine or glutamine affects the rate of intraprotein proton transfer in a most astonishing way; E166C exhibits the largest ratio, whereas with E166Q the ratio is smaller than that recorded for the WT protein (compare the results with Fig. 1 *C*).

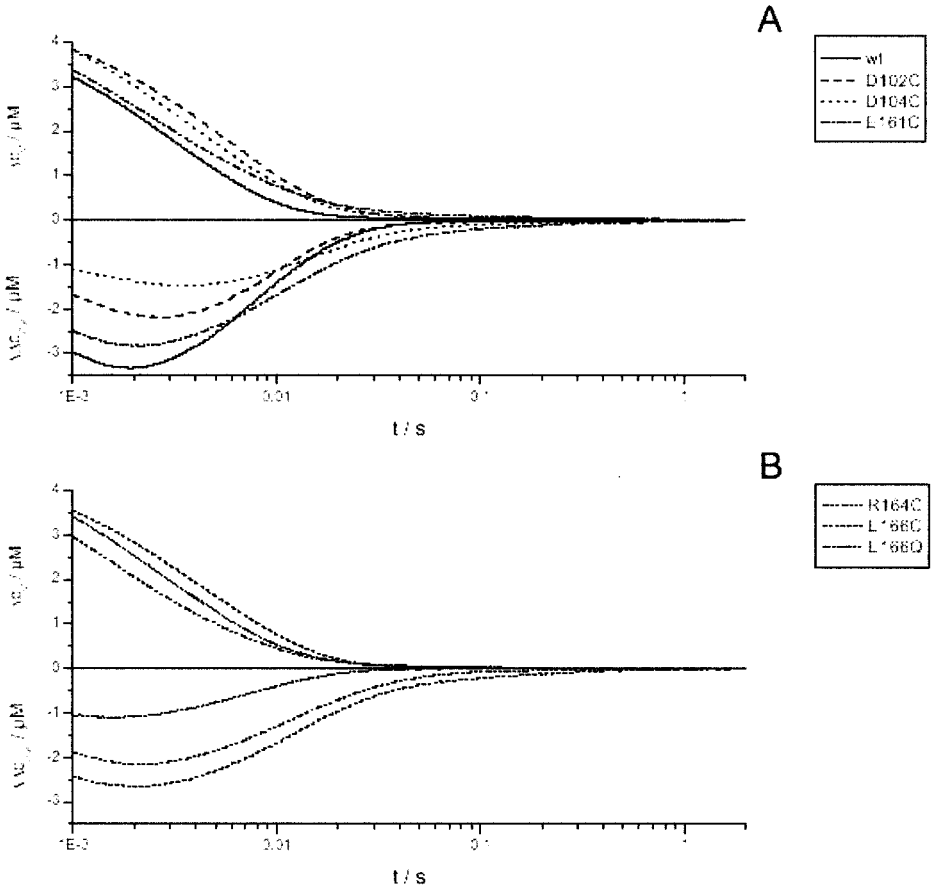

FIGURE 6 Flash-induced transient concentration changes of the M-intermediate at 412 nm (*upper traces*) and of pyranine (*lower traces*) in the aqueous bulk at 459 nm of WT bacteriorhodopsin and BR mutants D102C, D104C, and E161C (*A*), and of BR mutants R164C, E166C, and E166Q (*B*), in 150 mM KCl. The measurements were carried out at $T = 25°C$ and $pH = 7.5$.

DISCUSSION

In the present study we investigated the last phases of the photocycle, where the system relaxes through the uptake of bulk proton into the cytoplasmic section, compensating for the proton transferred to the Schiff base. To investigate the reaction mechanism, we had combined in this study two modes of observation. The first is the standard photo-cycle observation, where the transient absorbance of the retinal is used for quantitation of the state of protonation of the Schiff base, plus a parallel monitoring of the proton content in the bulk, using a pH indicator (pyranine) that does not adsorb to the negative surface of the purple membrane. This method allowed us to reconstruct, at any time, the balance of proton distribution between the Schiff base and the bulk. The second mode of observation was a fast kinetic recording of the proton transfer between the bulk and the surface of the protein, using a photo-excited pyranine for offsetting the bulk-surface equilibrium. The combination of the two modes allowed us to identify the rate-limiting steps associated with the reprotonation of the Schiff base.

The proton binding sites that are involved in this process are schematically presented in Scheme 1. At the beginning of the observation the Schiff base is deprotonated and, being the strongest base in the system, it regains a proton at the expense of the free proton in the bulk. The mechanism of proton delivery from the bulk to the Schiff base consists of at least four distinct steps that differ in their rate constants. The fastest one is the delivery of proton from the bulk to the surface of the protein, marked in Scheme 1 as a combination of a cluster and the carboxylate of D36 (Checover et al., 2001, 1997; Nachliel et al., 2002, 1997; Yaniv-Checover, 2002). The next carrier is the carboxylate moiety of D38, which is only partially exposed to the bulk, and most of the proton flux toward this carrier is through proton exchange reaction with the carboxylate of D36 (Checover et al., 1997; Nachliel et al., 2002). These reactions are fast and D38 equilibrates with the bulk within 10–200 μs. Thus, whatever was the cause for the slow proton transfer between the bulk and the Schiff base, it must be attributed to the intraprotein proton-transfer mechanism.

The slow propagation of the proton hole is observed as a temporal disequilibrium between the Schiff base and the bulk, where the residual of the proton binding capacity of the unprotonated Schiff base is smaller than the excess of protonated pyranine present in the bulk. The disequilibrium is manifested in a time frame that is order-of-magnitudes longer than the time constant of a bulk-surface proton exchange reaction.

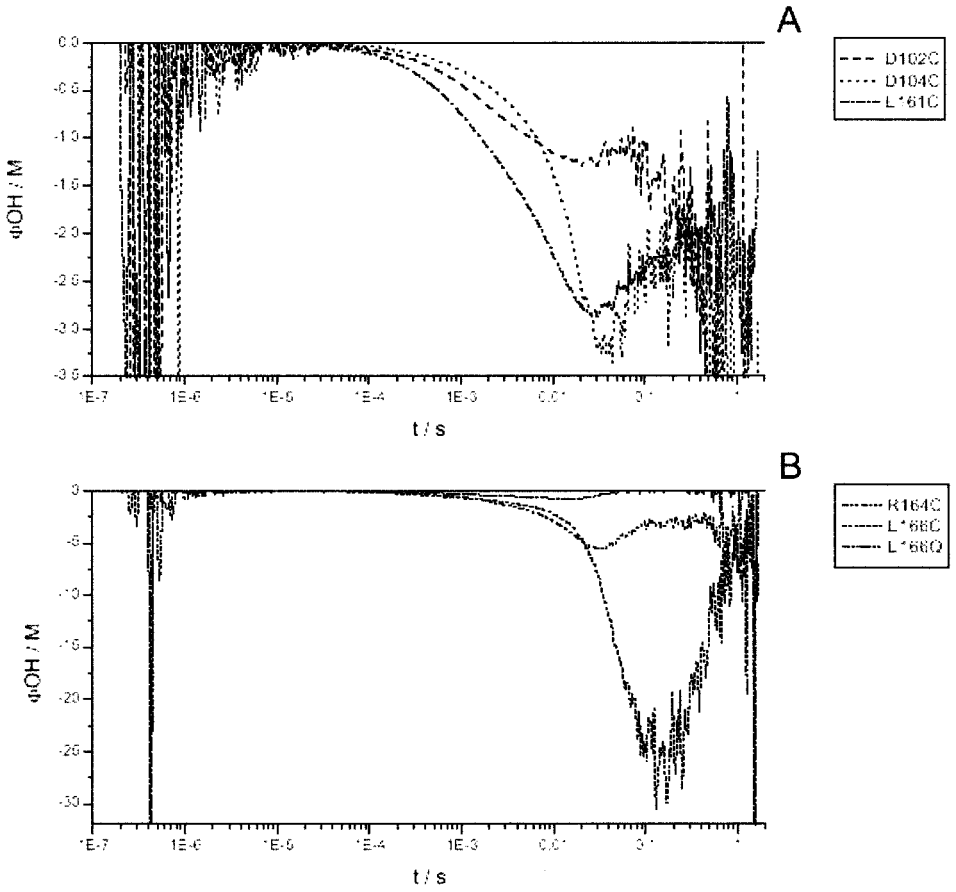

FIGURE 7 The variation of the ratio $\Delta\Phi OH_t/\Delta M_t$ as a function of time. The values were calculated from the data presented in Fig. 6.

The accepted mechanism of the catalytic cycle shows this transient disequilibrium as a state where D96 had already delivered a proton to the Schiff base but failed to be reprotonated by protons present in the bulk. Thus, the most relevant structure for our discussion should be a post-M intermediate (N or O) of the photocycle.

The passage of a proton from D38 to D96 takes place through a narrow opening that is located between the carboxylate of D38 and the positive charge of K41. The passage is illustrated using the O-like structure of Rouhani et al. (2001), 1jv7.pbd, where hydrogen atoms were added and the structure was relaxed by a brief minimization to release some Van der Waals interactions. As seen in Figure 8 *A*, the oxygen atom (*yellow*) of the carboxylate of D96 is partially exposed to the bulk through a narrow shaft ~10 Å deep that runs parallel to the hydrophobic surface of F42. The passage is too narrow to allow a water molecule to pass through, as evident by comparison with the two structural resolved water molecules (HOH512 and HOH523) located in the vicinity.

Fig. 8 *B* locates the shaft with respect to the structure of the protein. The presentation emphasizing the hydrophobic residues through which the proton hole is propagating. The carboxylate residue of D96 is colored in yellow and is partially covered by F42. A ring of hydrophobic residues surrounds the phenylalanine structure with a narrow leeway between them. Thus, a passage of a solvated proton across that plug will call for a concerted motion of the hydrophobic residues to make an opening large enough for the passage.

It should be pointed out that the shaft structure is not a unique feature of the O structure. It can easily be detected in the ground state structure of the 1brr.pdb file (Essen et al., 1998).

Fig. 9 is a longitudal section along the long axis of the protein extending from the cytoplasmic surface toward the Schiff base. The residues forming the hydrophobic collar and F42 are colored as in Fig. 8 *B*. The Schiff base and its proton donor (D96) are ~13 Å apart. Yet, the presence of water molecules in that space, observed in all post-M structures, render the passage of proton from D96 to Schiff Schiff base base to be faster than the hole propagation process described above. It is of interest to point out that for two mutations, D38C and R227Q, the M decay was extremely long, whereas the $\Delta\Phi OH_t/\Delta M_t$ ratios indicated no delay in the hole-propagation mechanism. Thus, we have to consider that some surface mutations can affect the dynamics of the proton transfer reaction in the D96-Schiff base section.

The carboxylate of D96 is totally inaccessible for free protons. The protonation of D96 happens by proton transfer from D38. The carboxylate moiety of D38 is reacting with

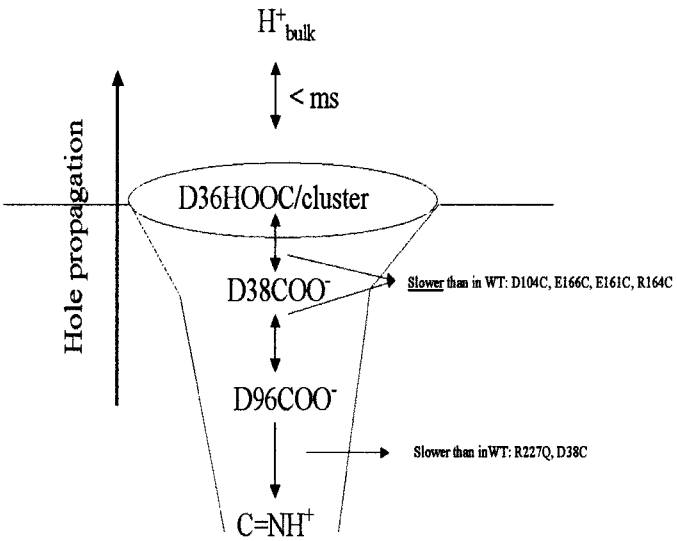

SCHEME 1 The proton-transfer reactions involved (in the presence of 150 mM KCl) in the second half of the catalytic cycle of bacteriorhodopsin and the steps whereby some mutants affect the overall rate of bulk-Schiff base equilibration. In all proteins the bulk-to-surface equilibration takes place in the submicrosecond time range and is never rate-limiting, not even in the mutant R227 with a 20-fold retarded reaction. In WT, the surface-to-D96 transfer limits the overall reaction and is further retarded in D104C, E166C, E161C, and R164C. In the mutants R227Q and D38C the rate of proton transfer from D96 to $C = N$ became the rate-limiting step.

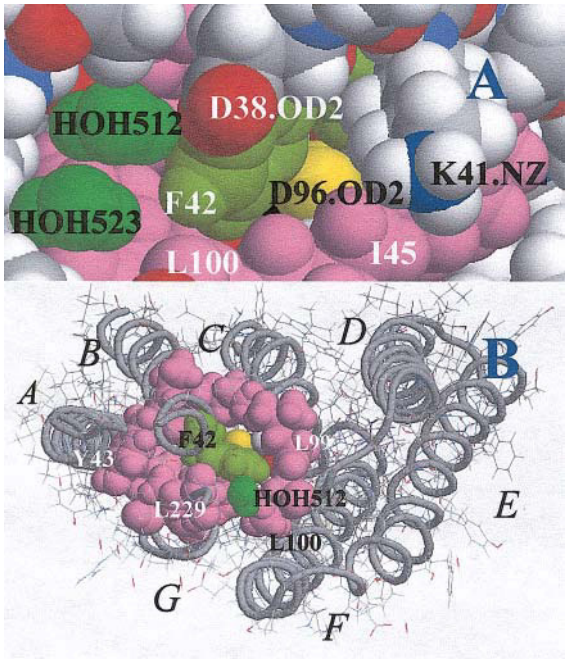

FIGURE 8 An expanded section of the cytoplasmic surface of bacteriorhodopsin (O-like structure; 1jv7.pdb; Rouhani et al., 2001, where hydrogen atoms were added and the structure was relaxed to release the Van der Waals interactions) emphasizing the detailed structure near the orifice of the hydrophobic gate. (*A*) Depicts the opening of the shaft through which the oxygen atom of the carboxylate moiety of D96 is exposed to the cytoplasmic surface. The shafts opens between the carboxylate of D38 and K41 and runs ~9-Å deep over the surface of F42. The shaft is too narrow to accommodate a water molecule, as can be deduced by comparison with the two x-ray resolved water molecules (*colored in green*) that are located close to the carboxylate of D38. (*B*) The protein is given by the helices structure plus wire frame, except of the residues making the hydrophobic gate using the same color code as in *A*. Please note the ring of hydrophobic residues that surrounds the shaft with F42 in its center.

free protons with a rate constant that is ~30% of the rate of protonation of a fully exposed residue (D36) and considered to be only partially accessible to the bulk.

The passage between the residues D38 and D96 is blocked by the bulky aromatic ring of F42, which is surrounded by a rim of hydrophobic residues. The space between F42 and the atoms of the nearby residues is in the order of 4–5 Å (*center to center*), which is too narrow to permit free passage of a water molecule. Indeed, the nearest stable site for a water molecule (HOH512, *colored green*) is not inside the hydrophobic domain and is located 3.5 Å from the carboxylate of D38. Thus, even though there seems to be an open path between the carboxylates of D96 and D38, the passage is too narrow to be permanently solvated. Accordingly, a passage of proton (or hydroxyl) between the two residues necessitates the overcoming of a high potential barrier associated with the insertion of a charge into a low dielectric matrix with a thickness of ~12 Å. A transient solvation of the domain will reduce the electrostatic barrier, but requires a major conformational change. For this reason we shall refer to the projected conducting pathway as a fracture zone, a site having a finite (but small) probability of temporal solvation.

Charge passage between D96 and D38

The passage of a charged particle from D38 to D96 proceeds through an ~12-Å thick hydrophobic slab, made by a large number of residues (P42, T46, A44, I45, L48, F72, L92, L95, L99, L100, T170, P171, and L223). It is of interest to note that this domain is even more resistant to solvent permeation than the D96→Schiff base section of the proton-conducting channel. In the BR ground state, the section between D96 and the Schiff base is devoid of water molecules, which accounts for the high pK of D96 (Cao et al., 1993; Zscherp et al., 1999). During the photocycle, following the translational motion of helix F in the M state of the protein, few water molecules (502, 503, and 504) are inserted between the carboxylate of D96 and the Schiff base. The introduction of these polarizable molecules into the hydrophobic space suffices to lower the pK of D96 from $pK > 12$ down to 7.1–7.5 (Zscherp et al., 1999; Szaraz et al., 1994; Dioumaev et al., 2001). In contrast, the section between the carboxylates of D96 and D38 remains unhydrated in the post-M states, retaining a low dielectric constant. As seen in Figs. 7 and 8, the domain between D38 and D96 is dominated by the aromatic structure of F42. When the residues surrounding F42 were replaced by smaller

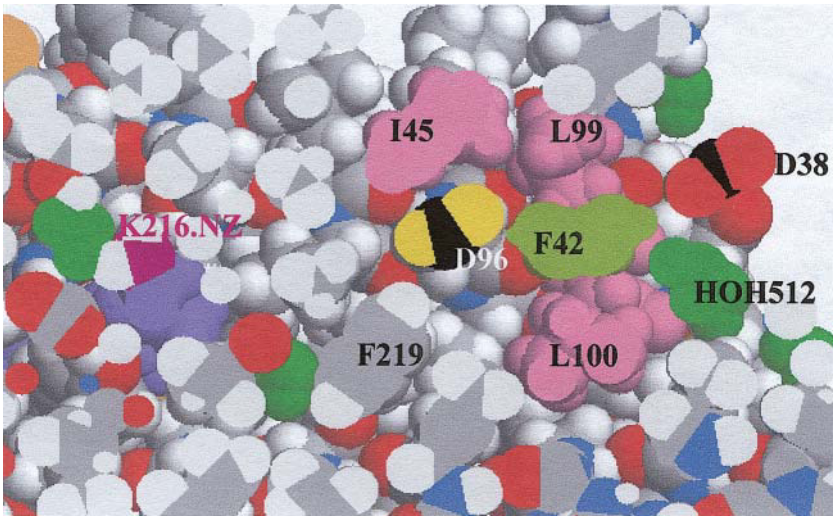

FIGURE 9 A cross-section along the bacteriorhodopsin emphasizing the trajectory of the hole propagation. The three proton-binding sites are marked in the figure. The Schiff base nitrogen (*purple*), and the carboxylates carbon atom of D96 and D38. The entrance to the hydrophobic gate is located between the carboxylate of D38 and K41 and extends over the two sides of F42 through a narrow passages between the benzene ring and the surrounding hydrophobic residues (colored in *gray*) that are 4–5 Å (*center to center*) from the benzene carbons. Considering the van der Waals radii, the passages are too narrow to allow water molecules to pass through.

ones (L100C, F171C, L223C, and F24C; see Dioumaev et al., 2001), the velocity of proton passage to D96 was even slower (Dioumaev et al., 2001). Apparently, the hydrophobic forces operating in the core of the protein are strong enough to let the structure collapse around the space vacated by the mutations. The replacement of a bulky residue by a smaller one allowed, on collapse, a better sealing of the passage and the reprotonation of D96 to be slowed down.

The rate-limiting step controlling the hole propagation

We can envision two mechanisms through which proton-hole migration takes place: *1*) The carboxylate of D96 hydrolyzes a nearby water molecule and the product, OH^- residue, diffuses toward the bulk. The slowness of the reaction is mostly attributed to the low rate of hydrolysis. *2*) The protonated carboxylate of D38 dissociates and the proton, instead of taking the most probable trajectory toward the bulk phase, is attracted by the negative charge of the ionized carboxylate of D96, causing it to penetrate into the fracture zone. In this case, the low frequency of the event is due to the high-energy barrier associated with charge entry into a low dielectric constant matrix.

The rate constant of the hydrolysis can be estimated using the relationship $k_h \sim 2 \times 10^{10} \times 10^{(pK-15.74)}$ (Gutman and Nachliel, 1990). Assuming that the *pK* of D96 in the post-M state is 7.1–7.5 (Dioumaev et al., 2001; Zscherp et al., 1999), the hydrolysis will occur once in ~25 ms, which is within the time frame of the hole-propagation process. Even though the approximation does not account for the specific conditions in the reaction site, such as the availability of the nearby water molecule, the hydrolysis appears to be sufficiently slow to account for the observed rate. A possible argument against this mechanism is based on the direction of the electrostatic forces inside the reaction space. Once D96 has donated its proton to the Schiff base, the hydroxyl will be attracted toward the positive charge of the Schiff base, interfering with the diffusion of the hydroxyl toward the bulk. Yet, the positive charge of K41, located at the exit of the shaft (11.2 Å from D96 and 6.4 Å from D38; see Fig. 8) may serve as an electrostatic attractor pulling the hydroxyl from the inside of the protein toward the surface.

The second mechanism is initiated by the spontaneous proton dissociation from the carboxylate of D38. The acceptance of this scenario is limited by the fact that the bulk is a preferred attractor for a free proton and the probability that the released proton will propagate through the hydrophobic gate is much smaller than the frequency of the carboxylate dissociation. The insertion of the proton into the protein can only take place when the fracture zone is temporarily solvated so that the combination of the attractive potential of the D96 anion plus the polarizability of the solvated shaft can effectively compete for the proton. Assuming that the diffusion coefficient of the proton (or the hydroxyl) within the hydrophobic barrier is smaller than in bulk water (Shimoni et al., 1993), then even a diffusion coefficient as small as 0.1% of the bulk value would yield a passage time of less than 1 ns.

Mutations affecting the rate of proton-hole propagation

The slow proton-hole propagation is a feature of the photocycle that was measured for the WT protein and for some mutants: D104C, E161C, R164C, and E166C. The fast kinetic measurements of bulk-surface proton transfer of the above mutants (Tables 1 and 4 above) indicated that the delay in the protonation of D96 could not be attributed to a slow proton transfer between bulk and surface. Even in the case of the purple membrane of the R227Q mutant, where the rate of proton exchange between the cluster and the

pyranine is 20-fold slower than that of the WT, it is not slow enough to impose a rate-limiting proton transfer step between the bulk and the protein's surface.

Four of the tested mutants (D38C, D102C, E166Q, and R227Q) failed to exhibit the slow-hole propagation. In the case of D38C and R227Q, the proton transfer from D96 to the Schiff base is the rate-limiting step of the relaxation, so that the reprotonation dynamics of D96 cannot be recorded. Yet, close examination of the pyranine deprotonation dynamics, measured with D38C in the presence of screening electrolyte, reveals some lengthening of its relaxation time (Table 2 *B*). This may be reminiscent of the slow-hole propagation mechanism that might be also operating in this protein.

In contrast to the above mutants, where the hole propagation cannot be observed due to the slow proton transfer from D96 to the Schiff base, the mutants E166Q and D102C exhibit a fast deprotonation of pyranine at a rate that kinetically matches the protonation of the Schiff base and no appreciable disequilibrium is detected. Apparently in some mutants the proton transfer between D38 and D96 can be faster than in the WT protein.

The effect of the screening electrolyte

The phenomenon recorded for the WT protein and some mutants was markedly enhanced when measured in the presence of a screening electrolyte. The effect of ionic screening on the electrostatic potential inside a membrane was elegantly discussed by McLaughlin (Mathias et al., 1992), who used a model of a low-dielectric slab immersed in an electrolyte solution. Their study showed that the ionic screening hardly affects the electrostatic potential at a distance shorter than the Debye length, κ^{-1}, that for a 150 mM KCl solution is 7.8Å. On the other hand, at distances exceeding κ^{-1}, the ionic screening affects the steepness of the electrostatic potential. Therefore, the forces operating on a mobile charge inside the protein are modulated by the screening electrolyte, affecting the velocity of intraprotein proton transfer reactions.

It should be emphasized that the addition of the screening electrolyte either increased the amplitude of ΦOH formation or in some cases (D102C, E166Q, and K159C) lowered it. The maximal concentration of ΦOH is determined by many parallel reactions that take place both inside the protein and at the bulk- protein interface and more than one of them can be affected by the electrolyte. Accordingly a general treatment of the correlation between the electrolyte and the amplitude of ΦOH is beyond the scope of the present study.

SUMMARY

The passage of a proton (or a hydroxyl) along the shaft connecting D96 with the cytoplasmic surface is a rare event that lasts a very short time. It most probably appears during random fluctuation of the protein, when the fracture zone opens up and a water molecule permeates inside. During this short ''period of grace,'' the proton or the hydroxyl can diffuse, driven by the local electric gradients generated by the charges of the Schiff base, and of D96, D38, and K41, which are located along the trajectory. Other charged residues make their contribution to the intraprotein electrostatic potentials and the ionic screening further modulates the local forces. Careful study of the hole propagation, combined with electrostatic mapping of the interior of the protein, may be a useful tool for understanding how the local forces control the motion of charges inside a protein.

This research is supported by the German-Israeli Foundation for Scientific Research and Development (Grant I –140-207.98 to M.G., N.A.D., and D.O.); the Israeli Science Foundation (Grant 427/01-1 to M.G.), Deutsche Forschungsgemeinschaft (Grant SFB 472), and Fonds der Chemischen Industrie (NAD).

REFERENCES

Cao, Y., G. Varo, A. L. Klinger, D. M. Czajkowsky, M. S. Braiman, R. Needleman, and J. K. Lanyi. 1993. Proton transfer from Asp-96 to the bacteriorhodopsin Schiff base is caused by a decrease of the pKa of Asp-96 which follows a protein backbone conformational change. *Biochemistry*. 32:1981–1990.

Checover, S., Y. Marantz, E. Nachliel, M. Gutman, M. Pfeiffer, J. Tittor, D. Oesterhelt, and N. A. Dencher. 2001. Dynamics of the proton transfer reaction on the cytoplasmic surface of bacteriorhodopsin. *Biochemistry*. 40:4281–4292.

Checover, S., E. Nachliel, N. A. Dencher, and M. Gutman. 1997. Mechanism of proton entry into the cytoplasmic section of the proton-conducting channel of bacteriorhodopsin. *Biochemistry*. 36:13919–13928.

Dencher, N. A., J. Heberle, G. Büldt, H.-D. Höltje, and M. Höltje. 1992. Active and passive proton transfer steps through bacteriorhodopsin are controlled by a light-triggered hydrophobic gate. *In* Structures and Functions of Retinal Proteins. J. L. Rigaud, editor. John Libbey Eurotext Ltd., Colloque, Paris, France. 221:213–216.

Dioumaev, A. K., L. S. Brown, R. Needleman, and J. K. Lanyi. 1999. Fourier transform infrared spectra of a late intermediate of the bacteriorhodopsin photocycle suggest transient protonation of Asp-212. *Biochemistry*. 38:10070–10078.

Dioumaev, A. K., L. S. Brown, R. Needleman, and J. K. Lanyi. 2001. Coupling of the reisomerizaton of the retinal, proton uptake, and reprotonation of Asp-96 in the N photo intermediate of bacteriorhodopsin. *Biochemistry*. 40:11308–11317.

Essen, L., R. Siegert, W. D. Lehmann, and D. Oesterhelt. 1998. Lipid patches in membrane protein oligomers: crystal structure of the bacteriorhodopsin-lipid complex. *Proc. Natl. Acad. Sci. USA*. 95:11673–11678.

Gerwert, K., B. Hess, J. Soppa, and D. Oesterhelt. 1989. Role of aspartate-96 in proton translocation by bacteriorhodopsin. *Proc. Natl. Acad. Sci. USA*. 86:4943–4947.

Gutman, M., and E. Nachliel. 1990. The dynamic aspects of proton transfer processes. *Biochim. Biophys. Acta*. 1015:391–414.

Gutman, M., and E. Nachliel. 1995. The dynamics of proton exchange between bulk and surface groups. *Biochim. Biophys. Acta*. 1231:123–138.

Lanyi, J. K. 1992. Reaction cycle and thermodynamics in bacteriorhodopsin. *Acta Physiol. Scand. Suppl*. 607:245–248.

Luecke, H., B. Schobert, J. P. Cartailler, H. T. Richter, A. Rosengarth, R. Needleman, and J. K. Lanyi. 2000. Coupling photoisomerization of retinal to directional transport in bacteriorhodopsin. *J. Mol. Biol*. 300:1237–1255.

Mathias, R. T., G. J. Baldo, K. Manivannan, and S. McLaughlin. 1992. Discrete charges on biological membranes. *In* Electrified Interfaces in Physics Chemistry and Biology. R. Guidelli, editor. Kluwer Academic Publishers. Dordrecht, Netherlands. 473–490.

Misra, S., R. Govindjee, T. G. Ebrey, N. Chen, J. X. Ma, and R. K. Crouch. 1997. Proton uptake and release are rate-limiting steps in the photocycle of the bacteriorhodopsin mutant E204Q. *Biochemistry*. 36:4875–4883.

Nachliel, E., Y. Finkelstein, and M. Gutman. 1996. The mechanism of monensin-mediated cation exchange based on real time measurements. *Biochim. Biophys. Acta.* 1285:131–145.

Nachliel, E., and M. Gutman. 1988. Time resolved proton-phospholipid interaction. Methodology and kinetic analysis. *J. Am. Chem. Soc*. 110:2629–2635.

Nachliel, E., M. Gutman, J. Tittor, and D. Oesterhelt. 2002. Proton Transfer Dynamics on the Surface of the Late M State of Bacteriorhodopsin. *Biophys. J*. 83:416–426.

Nachliel, E., S. Yaniv-Checover, and M. Gutman. 1997. The role of the surface group in funneling of protons towards the protonic channel of bacteriorhodopsin. *Solid State Ionics*. 97:75–82.

Oesterhelt, D., and L. Schuhmann. 1974. Reconstitution of bacteriorhodopsin. *FEBS Lett*. 44:262–265.

Pfeiffer, M., T. Rink, K. Gerwert, D. Oesterhelt, and H. J. Steinhoff. 1999. Site-directed spin-labeling reveals the orientation of the amino acid side-chains in the E-F loop of bacteriorhodopsin. *J. Mol. Biol*. 287: 163–171.

Rammelsberg, R., G. Huhn, M. Lubben, and K. Gerwert. 1998. Bacteriorhodopsin's intramolecular proton-release pathway consists of a -hydrogen-bonded network. *Biochemistry*. 37:5001–5009.

Richter, H. T., L. S. Brown, R. Needleman, and J. K. Lanyi. 1996. A linkage of the pKa's of asp-85 and glu-204 forms part of the reprotonation switch of bacteriorhodopsin. *Biochemistry*. 35:4054–4062.

Riesle, J., D. Oesterhelt, N. A. Dencher, and J. Heberle. 1996. D38 is an essential part of the proton translocation pathway in bacteriorhodopsin. *Biochemistry*. 35:6635–6643.

Rouhani, S., J. P. Cartailler, M. T. Facciotti, P. Walian, R. Needleman, J. K. Lanyi, R. M. Glaeser, and H. Luecke. 2001. Crystal structure of the D85S mutant of bacteriorhodopsin: model of an O-like photocycle intermediate. *J. Mol. Biol*. 313:615–628.

Sacks, V., Y. Marantz, A. Aagaard, S. Checover, E. Nachliel, and M. Gutman. 1998. The dynamic feature of the proton collecting antenna of a protein surface. *Biochim. Biophys. Acta*. 1365:232–240.

Shimoni, E., Y. Tsfadia, E. Nachliel, and M. Gutman. 1993. Gaugement of the inner space of the apomyoglobin's heme binding site by a single free diffusing proton. I. Proton in the cavity. *Biophys. J*. 64:472–479.

Szaraz, S., D. Oesterhelt, and P. Ormos. 1994. pH-induced structural changes in bacteriorhodopsin studied by Fourier transform infrared spectroscopy. *Biophys. J*. 67:1706–1712.

Tanford, C. 1957. The location of electrostatic charges in Kirkwood's model of organic ions. *J. Am. Chem. Soc*. 79:5348–5352.

Tanford, C., and R. Roxby. 1972. Interpretation of protein titration curves. Application to lysosyme. *Biochemistry*. 11:2192–2198.

Varo, G., and J. K. Lanyi. 1991a. Kinetic and spectroscopic evidence for an irreversible step between deprotonation and reprotonation of the Schiff base in the bacteriorhodopsin photocycle. *Biochemistry*. 30: 5008–5015.

Varo, G., and J. K. Lanyi. 1991b. Thermodynamics and energy coupling in the bacteriorhodopsin photocycle. *Biochemistry*. 30: 5016–5022.

Yaniv-Checover, S. 2002. Structure Function Relationship of Proton Transfer System on the Surface of Bacteriorhodopsin. Ph.D. thesis. Tel Aviv University, Tel Aviv, Israel.

Zscherp, C., R. Schlesinger, and J. Heberle. 2001. Time-resolved FT-IR spectroscopic investigation of the pH-dependent proton transfer reactions in the E194Q mutant of bacteriorhodopsin. *Biochem. Biophys. Res. Commun*. 283:57–63.

Zscherp, C., R. Schlesinger, J. Tittor, D. Oesterhelt, and J. Heberle. 1999. In situ determination of transient pKa changes of internal amino acids of bacteriorhodopsin by using time-resolved attenuated total reflection Fourier-transform infrared spectroscopy. *Proc. Natl. Acad. Sci. USA*. 96:5498–5503.